JOURNAL OF GEOPHYSICAL RESEARCH, VOL. 114, C07025, doi:10.1029/2008JC004791, 2009

Three-dimensional modeling of tide-induced suspended transport of seabed multicomponent sediments in the eastern English Channel

Nicolas Guillou,[1] Georges Chapalain,[1] and Laurent Thais[2]

Received 29 February 2008; revised 10 March 2009; accepted 12 May 2009; published 24 July 2009.

[1] A three-dimensional primitive numerical model is developed to simulate the circulation and resuspension of noncohesive sediments in the eastern English Channel. The present model is based on Coupled Hydrodynamical-Ecological Model for Regional and Shelf Seas (COHERENS) adapted for computing advection-diffusion of suspended multicomponent sediments. A statistical approach is first applied to interpolate spatial sampled grain size distributions with 11 classes at the computational grid nodes. These data then provide the availability of each class of sediment to be suspended. Finally, they are used to compute different bottom roughness parameters. Time histories of mean current and turbulent variables predicted by the model are compared with field data collected in two shallow sites off Hardelot and Merlimont beaches, in the south of Boulogne-sur-Mer (Dover Strait). Comparison of predicted and measured time histories of total suspended sediment concentration (SSC) is conducted at the Hardelot site. The model is used to quantify the respective contributions of SSC of the three grain size classes to resuspension processes. The spatiotemporal evolutions of the different classes in the surrounding area show local and advection-dispersion controlled remote suspension, both dependent on spatial changes in bathymetry, sediment composition, and coastline geometry.

Citation: Guillou, N., G. Chapalain, and L. Thais (2009), Three-dimensional modeling of tide-induced suspended transport of seabed multicomponent sediments in the eastern English Channel, *J. Geophys. Res.*, *114*, C07025, doi:10.1029/2008JC004791.

1. Introduction

[2] The Dover Strait is the narrow passage of 34 km wide connecting the eastern English Channel with the southern North Sea (Figure 1). In this area, moderate depths, averaging at 40 m, combined with the bottleneck of the English Channel, are known to produce extremely strong tidal currents reaching 1.7 m s^{-1} near the surface off cape Gris-Nez [*Service Hydrographique et Océanographique de la Marine*, 1973]. The area is also subject to occasional high storm activity [e.g., *Grochowski and Collins*, 1994]. The hydrodynamic climate makes the Dover Strait a region of intense bed erosion and sediment transport.

[3] Many models have been implemented over this area to gain a further insight of sediment transport processes [e.g., *Eisma and Kalf*, 1979; *Lafite et al.*, 2000; *Grochowski et al.*, 1993a, 1993b].

[4] However, these studies remained mainly confined to the bidimensional (2-D) transport of a single sedimentary class. Except works conducted by *Souza et al.* [2007] on native sediment transport, three-dimensional (3-D) modeling of sediment transport over this area have been focused on the input of very fine sediments (with median sieve diameter $d_{50} < 10$ μm) through river discharges [e.g., *Luyten et al.*, 1999b].

[5] The purpose of the present study is to numerically investigate tidal resuspension and transport of multisized bed materials in the eastern English Channel and its adjacent shallow water areas. Meteorological effects (atmospheric pressure gradient, wind driven circulation and surface gravity waves) as well as hydrological forcings are not considered in the present study. The novel aspect is that we deal with the resuspension and transport of the available amount of movable bottom sediments. The practical implication for modeling is that the real surficial sediment granulometric distribution must be used.

[6] The model application is illustrated by comparing with observational studies conducted in the south of Boulogne-sur-Mer by *Chapalain et al.* [1999] and *Chapalain and Thais* [2000], at two shallow sites off Hardelot and Merlimont beaches (Figure 1) during September 1997.

[7] The paper is organized as follows. The hydrodynamic and sediment transport model is described in section 2. In section 3, the model is applied to the study area. Emphasis is placed on the way to provide the actual grain size distribution of surficial sediments at the points of the computational grid (section 3.2). Predicted synoptic fields of near–free surface suspended sediment concentration (SSC) are provided (section 3.3). Point predictions are then compared with

[1] Laboratoire Génie Côtier et Environnement, Département Environnement Littoral et Cours d'Eau, Centre d'Etudes Techniques Maritimes et Fluviales, Plouzané, France.

[2] Laboratoire de Mécanique de Lille, UMR 8107, USTL, Polytech'Lille, CNRS, Villeneuve d'Ascq, France.

0148-0227/09/2008JC004791$09.00

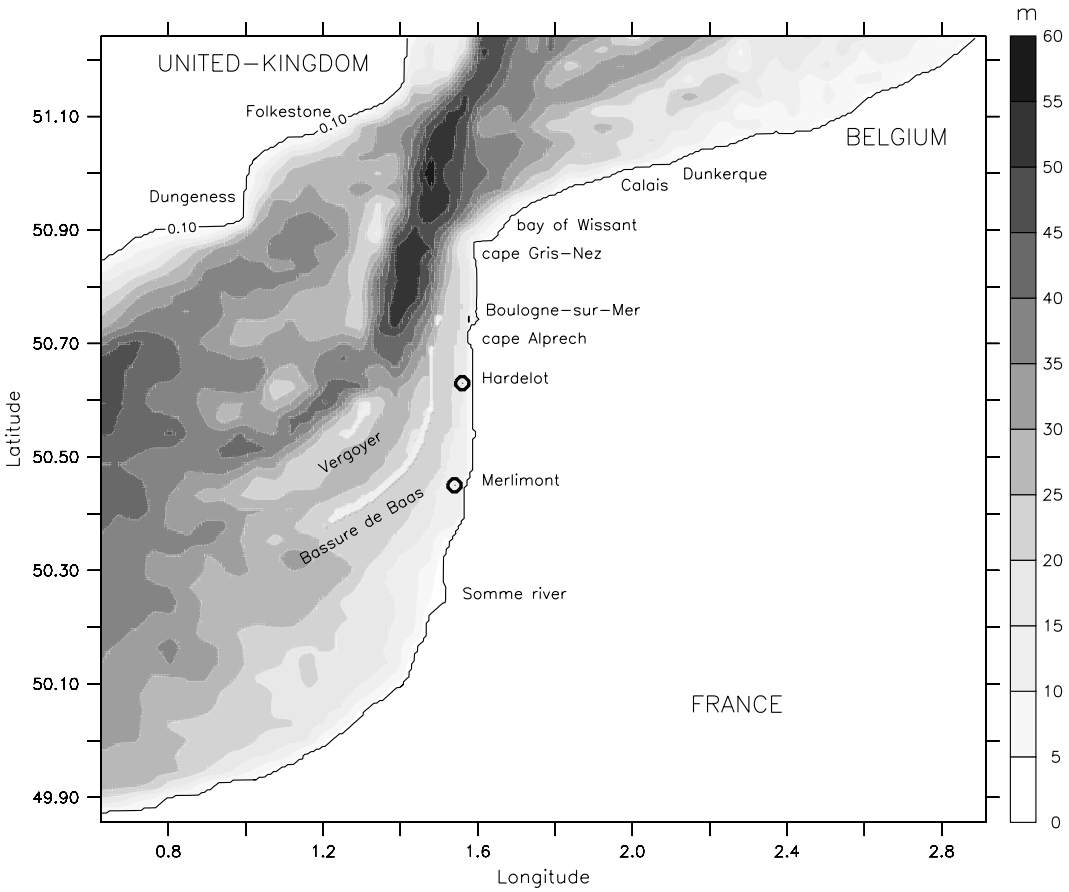

Figure 1. Bathymetry of the Dover Strait taking into account the mean sea level.

field data (section 3.4). Finally the contribution of each sedimentary classes to the SSC signal at the Hardelot site is further investigated (section 4). Conclusions are drawn in section 5.

2. Model

2.1. Assumptions

[8] The flow is assumed to be turbulent over a rough bottom characterized by the roughness parameter z_0 defined as the height above the bottom at which the fluid velocity is zero. On featureless bottoms, this parameter is related to the grain size diameter $z_0 = d_{90}/10$ [*Van Rijn*, 1993] with d_{90} the grain diameter of the bottom sediments for which 90% of the grains by mass is finer. On sandy beds with median diameters $d_{50} < 800$ μm [*Soulsby*, 1997], ripples are ubiquitous with a height $\eta_r = 100 d_{50}$ and a wavelength $\lambda_r = 1000 d_{50}$ [*Yalin*, 1985]. In this case, the roughness parameter is given by the semiempirical relationship of *Wooding et al.* [1973] $z_0 = 2\ \eta_r\ (\eta_r/\lambda_r)^{1.4}$.

[9] The sedimentary particle assemblage is treated as a number of polydispersive components of different grain sizes. Individual particles are assumed to be spherical, noncohesive and made of quartz with density ρ_s equal to 2650 kg m^{-3}. Additional constraints must be placed upon the particle size in order to ensure that the fluid-sediment mixture retains the Newtonian behavior of a clear fluid [*Grant and Glenn*, 1983]. It is therefore assumed that the smallest length scale of the turbulence is large in comparison with the largest particle size [*Barenblatt*, 1953]. For a typical friction velocity $u^* \sim 10^{-2}$ m s^{-1} in the eastern part of the English Channel, the dissipation rate is of order $\varepsilon \sim 2 \times 10^{-6}$ m^2 s^{-3}, which corresponds to a Kolmogorov microscale of turbulence $l_\kappa \sim 800$ μm. This can be safely considered as large compared with the largest particles likely to move in suspension under average tidal conditions. It is also supposed that the particle concentration is high enough to represent a continuum, but low enough to neglect particle interactions (<8 g l^{-1}) [*Lumley*, 1978]. It is further assumed that the inertia of the particles is small [*Soo*, 1967; *Lumley*, 1978], so that except for a systematic constant settling velocity, the particles follow the mean flow. The effects of stratification due to suspended sediments are thus neglected on the basis of the criterion of *Soulsby and Wainwright* [1987]. Typical conditions encountered in the study area fall under regime I where stratification is insignificant. The water-sediment mixture is thus assumed homogeneous with a density $\rho = 1025$ kg m^{-3} corresponding to clear water with a temperature $T = 10$°C and a salinity $S = 35$ psu, practical salinity units.

2.2. Model Description

[10] Many 3-D models based on the above listed assumptions have been developed [e.g., *Sheng*, 1983; *Hess*, 1986; *Blumberg and Mellor*, 1987; *Schepetkin and McWilliams*, 2005]. Here we choose the primitive equation model COHERENS (Coupled Hydrodynamical-Ecological Model for Regional and Shelf Seas) [*Luyten et al.*, 1999a] supple-

mented with a multicomponent SSC transport module adapted from its existing sediment transport module.

2.2.1. Hydrodynamic Equations

[11] The hydrodynamic module of COHERENS solves the time-averaged continuity equation and horizontal momentum equations derived using the Boussinesq approximations and the vertical hydrostatic equilibrium on a spherical σ coordinate system. The horizontal eddy viscosity ν_H and diffusivity λ_H are parameterized following *Smagorinsky* [1963]. The vertical eddy viscosity ν_T and eddy diffusivity λ_T are expressed according to *Luyten et al.* [1996] in terms of the turbulent kinetic energy k and its dissipation rate ε obtained by solving a standard two-equation $k-\varepsilon$ turbulence closure scheme [e.g., *Launder and Spalding*, 1974; *Rodi*, 1984]. Further details about the hydrodynamic module, its boundary conditions as well as its numerical resolution are given by *Luyten et al.* [1999a].

2.2.2. SSC Equations

[12] The volumetric concentration C_i of each individual class subscripted i, with $1 \le i \le N_p$ and N_p the number of classes considered, is interpreted as an arbitrary scalar quantity satisfying the transport equation

$$\frac{\partial HC_i}{\partial t} + \nabla.(HC_i\mathbf{u}) + \frac{\partial}{\partial\sigma}[(\tilde{w}-w_{si})C_i] = \frac{\partial}{\partial\sigma}\left(\frac{\lambda_T}{H}\frac{\partial C_i}{\partial\sigma}\right) + \nabla.(H\lambda_H\nabla(C_i)) \quad (1)$$

where $\mathbf{u}$ is the horizontal velocity component, $\tilde{w}$ is the vertical velocity normal to σ planes, t denotes time, ∇ is the horizontal gradient operator and finally H is the total water depth. The transport equation is intended to convey the physical basis for particles falling under their own weight with a settling velocity w_{si}, and being advected and diffused by the current. The settling velocity is prescribed for each class of particle diameter according to *Soulsby*'s [1997] formulation

$$w_{si} = \frac{\nu}{d_i}\left[\left(10.36^2 + 1.049D_{*i}^3\right)^{1/2} - 10.36\right] \quad (2)$$

with

$$D_{*i} = \left[\frac{g(s-1)}{\nu^2}\right]^{1/3} d_i \quad (3)$$

the dimensionless grain size where d_i is the grain size diameter of the class considered, g is the gravity acceleration, $\nu = 1.36 \times 10^{-6}$ m^2 s^{-1} is the molecular viscosity of sea water at 10°C and 35 psu and $s = \rho_s/\rho$.

[13] At the free surface, a zero flux condition is imposed

$$w_{si}C_i + \frac{\lambda_T}{H}\frac{\partial C_i}{\partial\sigma} = 0 \quad (4)$$

while the boundary condition at the lower limit of integration of the sediment laden flow is prescribed as the net volumetric flux of sediments through the water-sediment interface

$$w_{si}C_i + \frac{\lambda_T}{H}\frac{\partial C_i}{\partial\sigma} = D_i - E_i. \quad (5)$$

This flux is the difference between the downward deposition rate D_i due to settling of particles and the upward entrainment rate of sediments from the seabed E_i. The deposition rate is simply expressed as

$$D_i = w_{si}C_i^{bot} \quad (6)$$

where C_i^{bot} is the near-bed SSC [e.g., *Lick*, 1982; *Lavelle et al.*, 1984; *Chapalain and Thais*, 2000].

[14] The method used here to specify the entrainment rate E_i follows *Van Rijn* [1986], *Celik and Rodi* [1988, 1991], and *Chapalain and Thais* [2000]. It is based on the physical hypothesis that the flow always entrains as much sediment from the seabed as it can with the energy available. This implies that, for a situation with a loose bed of unlimited sediment material supply, the entrainment always occurs as its maximum rate. This entrainment rate of sediment class i under full capacity equilibrium situation (i.e., zero net flux across the bottom corresponding to a balance between deposition and entrainment) is

$$E_i = w_{si}C_i^{ref}. \quad (7)$$

The maximum equilibrium near-bed reference SSC C_i^{ref} in equation (7) is given by the semiempirical expression of *Smith and McLean* [1977],

$$C_i^{ref} = f_i C_b\left[\frac{\gamma_0 T_{si}}{1+\gamma_0 T_{si}}\right], \quad (8)$$

where f_i is the availability for resuspension of sediments in size class i taken equal to the percentage of bed sediments in this class provided by the grain size analysis, $C_b = 0.65$ is the total volume concentration of sediment in the settled bed ($C_b = 1 -$ porosity), γ_0 is an empirical resuspension parameter and T_{si} is the local normalized excess skin shear stress for class i

$$T_{si} = \mathrm{Max}\left[\frac{\tau_{skin}-\tau_{cri}}{\tau_{cri}}; 0\right], \quad (9)$$

with τ_{skin} the skin shear stress exerted on the bottom and τ_{cri} its critical value of motion of sedimentary particles of class i. Ignoring armoring effects, τ_{cri} is computed with *Soulsby and Whitehouse*'s [1997] formulation

$$\tau_{cri} = g(\rho_s-\rho)d_i\theta_{cri} \quad (10)$$

with

$$\theta_{cri} = \left[\frac{0.30}{1+1.2D_{*i}} + 0.055\left[1-\exp\left(-0.020D_{*i}\right)\right]\right]. \quad (11)$$

On featureless seabeds, the skin shear stress τ_{skin} equals the fluid shear stress $\tau_b = \rho\, u_{*b}^2$. On rippled sandy beds, following *Li*'s [1994] empirical works, the spatially averaged skin shear stress is given by

$$\tau_{skin} = \tau_b\left[\alpha\left(u_{*b}/\eta_r\right) + \beta\right]^2 \quad (12)$$

with

$$(\alpha,\beta)=\begin{cases}(0.125\ \mathrm{s},0.373) & \text{for}\quad u_{*b}/\eta_r<2.3\ \mathrm{s}^{-1}\\ (0.107\ \mathrm{s},0.266) & \text{for}\quad u_{*b}/\eta_r\geq 2.3\ \mathrm{s}^{-1}.\end{cases}\qquad(13)$$

2.2.3. Numerical Method

[15] The numerical method keeps the COHERENS schemes for space and time discretizations of hydrodynamic and SSC equations [*Luyten et al.*, 1999a]. Only two modifications have been implemented in the present version of the model. The first modification concerns the implementation of a one-way nested grid approach with a fine and complete (hydrodynamic and hydrosedimentary processes computation) resolution inner model embedded inside a coarse-resolution outer model restricted to hydrodynamic computations. The sea level is imposed along the open boundaries of the outer domain. The mean velocities normal to these boundaries result from *Blumberg and Kantha*'s [1985] implicit condition. Computed free surface and currents are then prescribed on the open boundaries of the inner domain. The mean velocities along the boundaries of the inner domain are derived from an iterative scheme which minimizes wave reflection [*Flather*, 1976]. The three-dimensional velocities normal to the open boundaries of the outer and inner domains are imposed with the help of a simple radiation condition [*Blumberg and Mellor*, 1987]. Finally, zero tangential velocity components are used on the outer boundaries both for the internal and external modes. The second modification deals with the implementation of a fine resolution near-bed method in order to improve the computation of SSC and deposition rates at the water-sediment interface. In a region of exponential growth of the SSC magnitude, a close estimate of the deposition rate and the near-bed SSC C_i^{bot} is required. Using an uniform vertical σ mesh for hydrodynamics and SSC transport equation resolution results in an underestimation of the deposition rate at the first vertical COHERENS σ grid point above the bottom and an overestimation of the total SSC. The present method improves these numerical results. It consists in nesting a 7-level submodel between the bottom and the first vertical σ grid point. Analytical solutions based on the law of the wall are used for hydrodynamic variables (namely, velocity components, eddy viscosity and diffusion coefficients). In contrast, SSC equations are numerically solved through the entire water column, from the lower nested grid point to the upper grid point near the free surface. This approach avoids matching problems particularly tedious during deposition phases around slack waters. Further details on this present submodel are given by *Guillou* [2007].

3. Model Application and Results

3.1. Grid Arrangement and Boundary Conditions

[16] The outer computational domain extends in longitude from 3.000°W to 4.700°E and in latitude from 48.560°N to 52.850°N while the inner domain extends from 0.626°E to 2.914°E and 49.856°N to 51.242°N (Figure 2). These domains are discretized on a 260 × 239 horizontal regular grid with a resolution of 2 km and a 309 × 309 horizontal regular grid with a mesh size of 500 m. The outer model has 10 uniform vertical grid cells. The inner model has 11 uniform vertical grid cells completed with 7 above-mentioned near-bed sublayer cells. The time steps for the external modes are 20 and 10 s for the outer and inner models, respectively. The time step for the internal mode is 200 s for both models.

[17] The bathymetry is linearly interpolated from the data used by *Salomon et al.* [1993]. In the outer domain, the bottom roughness parameter is set to z_0 = 0.0035 m according to *Luyten et al.* [1999b]. In the inner domain where the bottom sediment distributions are introduced (see section 3.2), z_0 is parameterized taking the presence of ripples into account (section 2.1).

[18] The outer model is driven by the dominant 21 tidal constituents extracted from a long-term run of the 2-D COHERENS model on the northwest European continental shelf (J. Ozer, Management Unit of the North Sea Mathematical Models, personal communication, 1999). The tidal signal predicted every 10 min at 15 points along each open boundary is interpolated at all grid points and every time step using a cubic spline.

3.2. Grain Size Distributions

[19] A series of 679 bottom sediment samples was collected in the inner domain (Figure 3a) from 1971 to 1976 in the framework of the RCP 378 Benthos de la Manche program [*Cabioch et al.*, 1977]. Each sample was passed through a series of 9 standard AFNOR sieves ranging from 50 μm to 2 cm (Table 1). A virtual class between 30 cm and 1 m is added to account for boulders and rocky outcrops. Finally, 11 classes are considered with a finest grain size diameter d_1 = 25 μm. The method of *Leprêtre et al.* [2006] combining the use of Spherical Factor Analysis (SFA) and kriging is applied to determine the grain size distributions (i.e., f_i in equation (8)) at the grid nodes of the inner domain. The map of the median sieve diameter computed (Figure 3a) reproduces fairly well the sediment pattern established by sedimentologists [e.g., *Vaslet et al.*, 1979; *Augris et al.*, 1987] and characterized by (1) large sandy areas in the eastern English Channel and the southern North Sea exhibiting prominent sandbanks like the Bassure de Baas or the Vergoyer off Hardelot, (2) gravel and pebble deposits in the Dover Strait where tidal currents are the strongest, and (3) silty and muddy sediments concentrated in the inner shelf. From the equality between the skin shear stress τ_{skin} computed by the model and critical shear stress τ_{cr}, it is possible to have an estimate of the critical diameter below which bottom sediments are undisturbed by the flow. Figure 3b shows the map of the critical diameter inferred from the highest tidal shear stress constraints in the inner domain. Comparison between Figures 3a and 3b suggests that the sediment of the Dover Strait are being arranged by tidal currents. This causal relationship has been proposed and described at the scale of the whole English Channel mainly by *Stride* [1963], *Kenyon and Stride* [1970] and *Stride et al.* [1972].

3.3. Predicted Synoptic Fields of Near–Free Surface Total SSC

[20] Figure 4 displays the predicted synoptic fields of total SSC at 40 cm below the free surface at flow peaks and slack waters in the center of the inner domain (λ = 1.400°E,

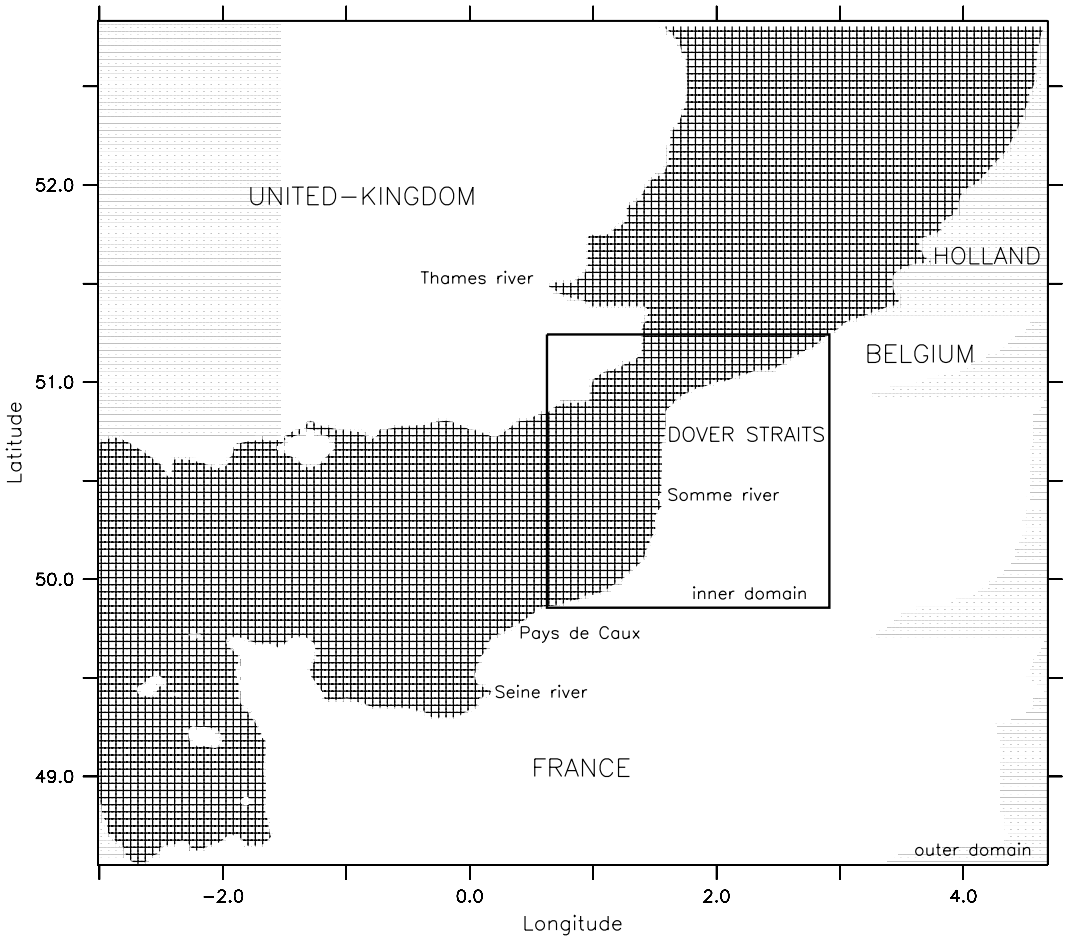

Figure 2. Outer and inner computational domains.

ϕ = 50.900°N) for a mean tidal cycle. Different spots appear seaward the English coast, off Dungeness and Folkestone and the French coast, off Dieppe and the bay of Somme, in the south of Boulogne-sur-Mer and off Calais. As tide-induced turbulence and resuspension are very active during flow peaks (t2 and t4), the resuspension spots expand particularly seaward the Kent with an excrescence in the Dover Strait while they diminish and even disappear off the bay of Wissant as above processes weaken with respect to sedimentation around slack waters (t1 and t3). A marked flood related spot develops in the lee of cape Gris-Nez (t2). In the central eastern channel, two permanent spots arise on the top of the Bassure de Baas and Vergoyer sandbanks where very silty sand (d_1 = 25 μm) are available.

3.4. Comparisons With Point Measurements

3.4.1. Experiment Description

[21] Measurements here used were made at two sites in the eastern English Channel. The first site is located off Hardelot beach, at longitude 1.555°E and latitude 50.633°N in mean water depth of 16.5 m. The second measuring point is situated off Merlimont beach at longitude 1.537°E and latitude 50.450°N in mean water depth of 13.5 m (Figure 1). The tidal period is semidiurnal (T = 12.4 h) with a spring tide range of 7 m. An echo sounder survey showed that the bottom in this area was featureless and flat. Bed sediments were collected at the two experimental sites. The bottom sediment at Hardelot is a silty sand with a median sieve diameter d_{50} = 225 μm comprising 11% silt and very fine sand, 48% fine sand, 28% medium sand, 5% coarse sand and 8% very coarse sand. The bed material at the Merlimont site is sand with a median sieve diameter d_{50} = 256 μm comprising 7% silt and very fine sand, 39% fine sand, 50% medium sand, 4% coarse and very coarse sand [*Chapalain and Thais*, 2000]. These data are consistent with those interpolated from the RCP 378 Benthos de la Manche data set (section 3.2) which exhibits the nearshore belt of bottom silty sand from Merlimont to Boulogne-sur-Mer (Figure 5).

[22] The instrumentation was deployed at the Hardelot site over the period 21–24 September 1997 and at the Merlimont site over the period 25–28 September 1997. These data sets are characterized by contrasting tidal conditions. The first

Figure 3. (a) Median sieve diameter expressed in the Wentworth's grain size scale $\Phi_{50} = -\log_2(d_{50})$ (with d_{50} in mm) in the inner domain. The inset represents the geographic distribution of the 679 RCP 378 Benthos de la Manche grab samples in the Dover Strait. (b) Critical incipient motion diameter in the Wentworth's scale inferred from the highest tidal conditions in the inner domain.

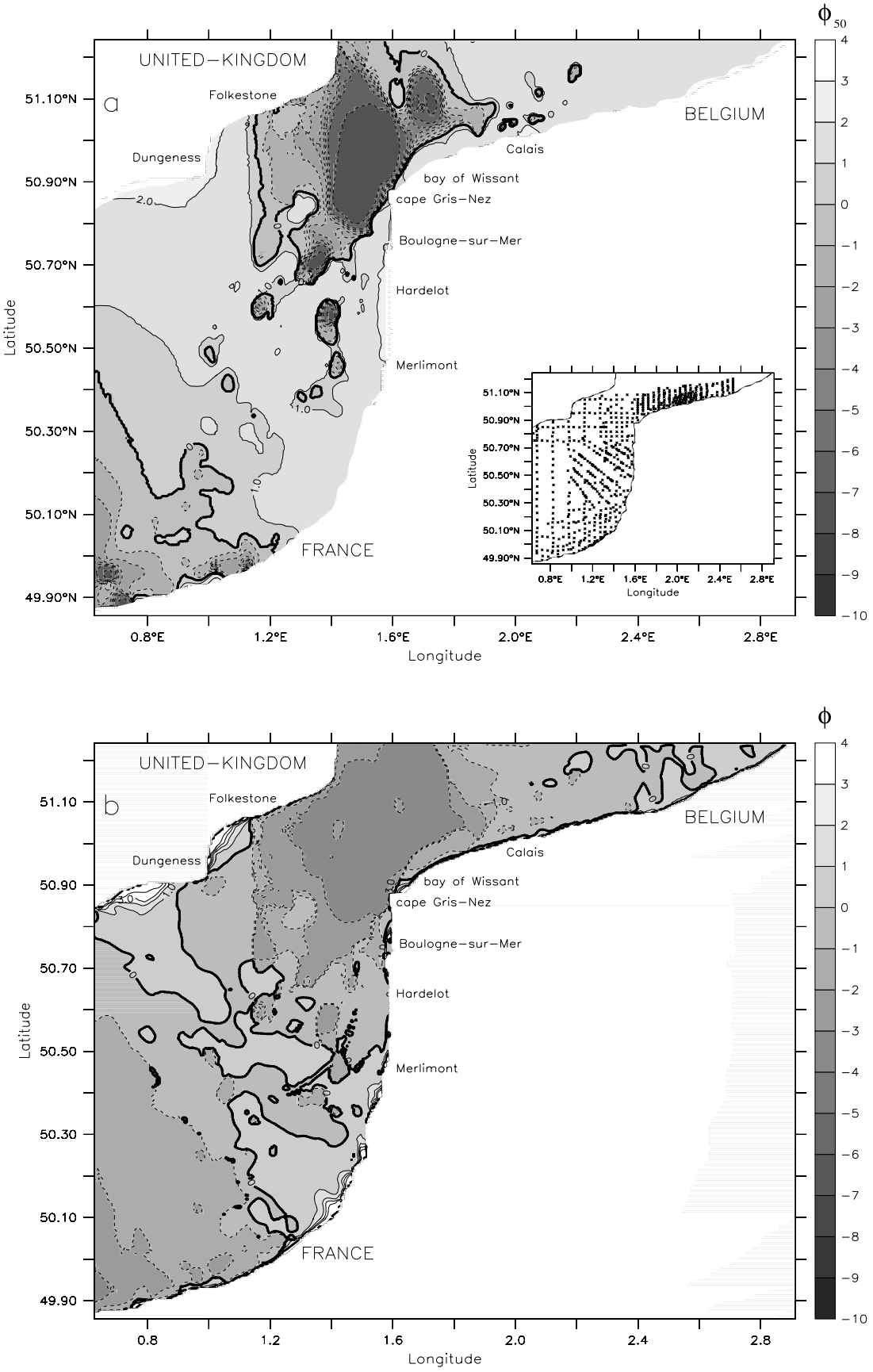
a
UNITED−KINGDOM
BELGIUM
FRANCE
Folkestone
Dungeness
Calais
bay of Wissant
cape Gris−Nez
Boulogne−sur−Mer
Hardelot
Merlimont
2.0
1.0
1.0
51.10°N
50.90°N
50.70°N
50.50°N
50.30°N
50.10°N
49.90°N
0.8°E
1.2°E
1.6°E
2.0°E
2.4°E
2.8°E
Latitude
Longitude
ϕ50
4
3
2
1
0
−1
−2
−3
−4
−5
−6
−7
−8
−9
−10
b
UNITED−KINGDOM
BELGIUM
FRANCE
Folkestone
Dungeness
Calais
bay of Wissant
cape Gris−Nez
Boulogne−sur−Mer
Hardelot
Merlimont
1.0
51.10
50.90
50.70
50.50
50.30
50.10
49.90
0.8
1.2
1.6
2.0
2.4
2.8
Latitude
Longitude
ϕ

Figure 3

Table 1. Aperture Sizes of AFNOR Series of Sieves and Mean Grain Size Diameters of Corresponding Classes

Class	Standard Sieve Diameters	Grain Size Diameter d_i
1	0–50 μm	25 μm
2	50–100 μm	75 μm
3	100–200 μm	150 μm
4	200–500 μm	350 μm
5	0.5–1 mm	750 μm
6	1–2 mm	1.5 mm
7	2–5 mm	3.5 mm
8	0.5–1 cm	7.5 mm
9	1–2 cm	1.5 cm
10	2–30 cm	16 cm
11	0.3–1 m	65 cm

series of measurements at the Hardelot site occurred in a period of spring to neap tides, whereas the second series was characterized by neap to spring tides. Fair weather conditions prevailed during the experimental studies. The instrumentation system is a heavily weighted benthic tripod equipped with (1) an upward looking 1200 kHz Broad-Band Acoustic Doppler Current Profiler (BBADCP) manufactured by RD Instruments for current velocity and acoustic backscatter signal strength profiling of the outer boundary layer ($z > 4.5$ m above the bottom) with a vertical resolution of 1 m and temporal resolution of 5 min and (2) an instrument package resolving the inner boundary layer every half hour at a rate of 4 Hz in 9-min records and incorporating a Paroscientific pressure sensor located at $z = 2.17$ m above the bottom and a vertical array of four Marsh-McBirney 3.8 cm diameter electromagnetic current meters measuring the horizontal velocities at heights $z = 0.3$, 0.6, 0.9 and 1.4 m above the bottom. Data used here represent time series of burst averages. Because of a technical malfunction, two bursts are not validated at the Hardelot site on 22 September 1997. The turbulent kinetic energy is extracted from the raw kinetic energy and the current orbital wave contributions. A series of water samples were collected at 5 and 8 m above the bottom to establish calibration curves useful to calibrate the time series

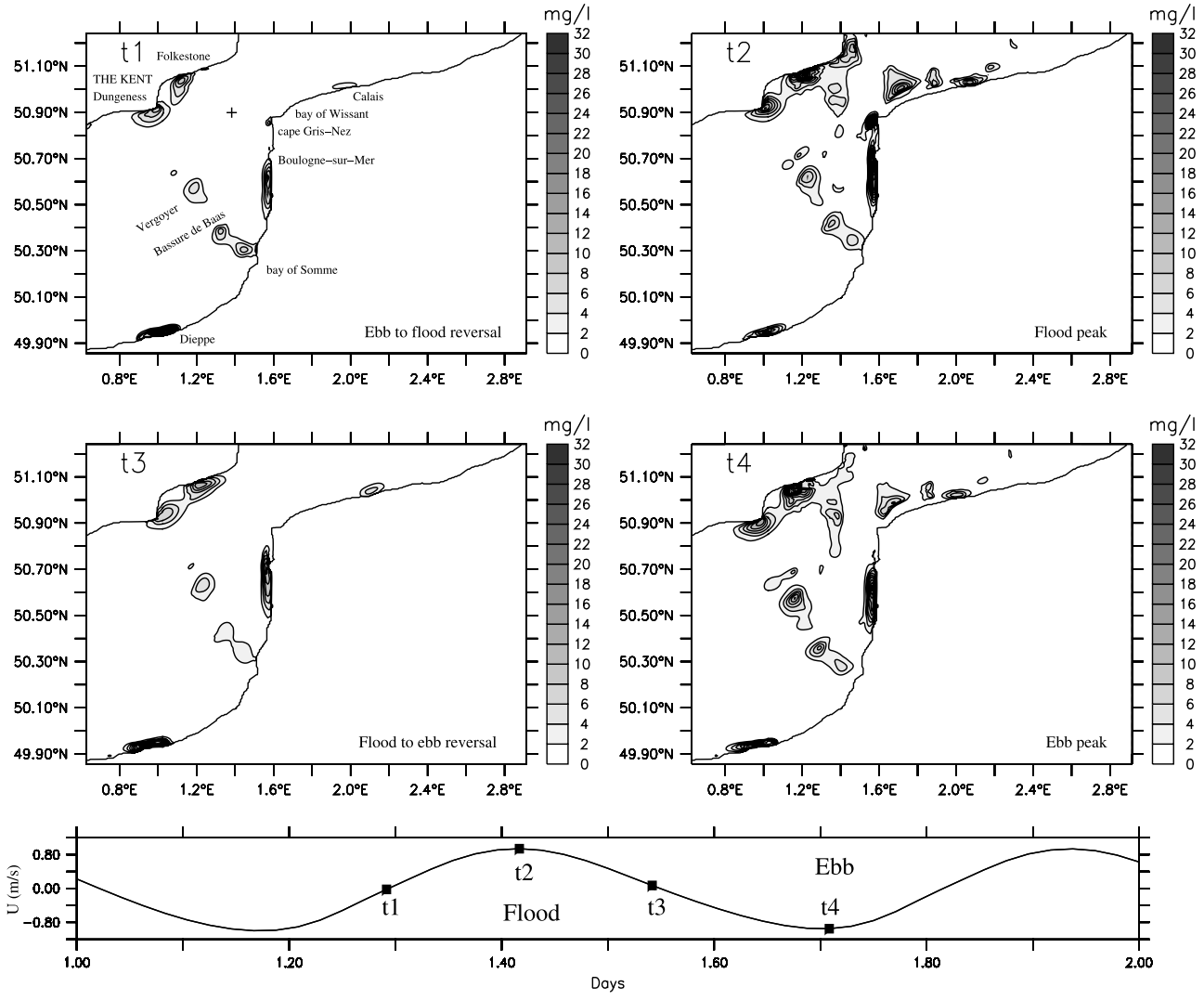

Figure 4. Predicted fields of total SSC 40 cm below the free surface at times of current peaks (t2 and t4) and slack waters (t1 and t3) of a mean tidal cycle in the center of the inner domain ($\lambda = 1.400°$E, $\phi = 50.900°$N), localized by a plus in the t1 plot.

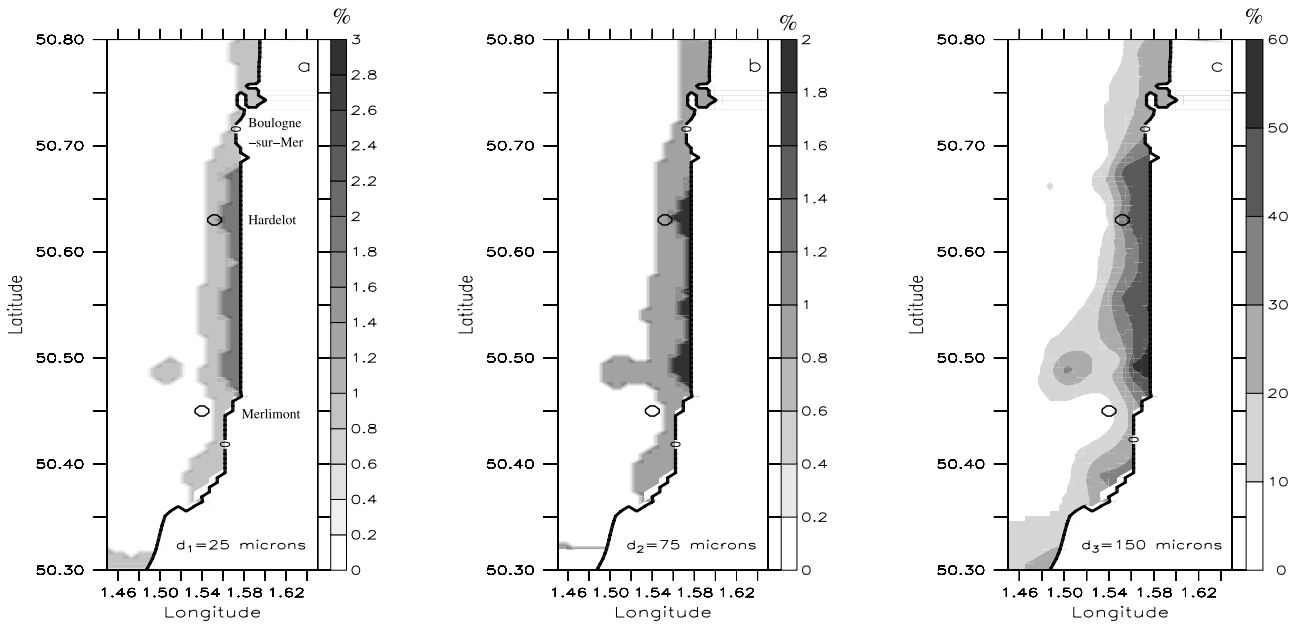

Figure 5. Proportions of each of the first three grain size classes in the surroundings of the Hardelot site: (a) d_1 = 25 μm, (b) d_2 = 75 μm, and (c) d_3 = 150 μm.

of BBADCP backscattered signal. More details about the data reduction procedure are given by *Chapalain et al.* [1999] and *Chapalain and Thais* [2000].

3.4.2. Hydrodynamic Predictions

[23] Figures 6 and 7 display the model predictions for the current speed and direction (clockwise from north) at 0.9 and 5 m above the bottom together with the measurements at the Hardelot and Merlimont sites. The origins of the time series at the Hardelot site (Figure 6) and the Merlimont site (Figure 7) correspond to 1415 UT on 21 September 1997 and 1755 UT on 25 September 1997, respectively. The current predominantly flows north and ebbs south almost parallel to the coastline. The temporal variation of the current around slack water appears slightly faster before flood than before ebb. An overall good agreement between measurements and predictions of currents is found at the two sites. A slight underestimation (15–20%) by the model of current speeds at 0.9 m above the bottom in the second half of the measurement period at the Merlimont site is noticed.

[24] Model predictions of the time series of the turbulent kinetic energy at z = 0.9 m above the bottom at the Merlimont and Hardelot sites are plotted with measurements

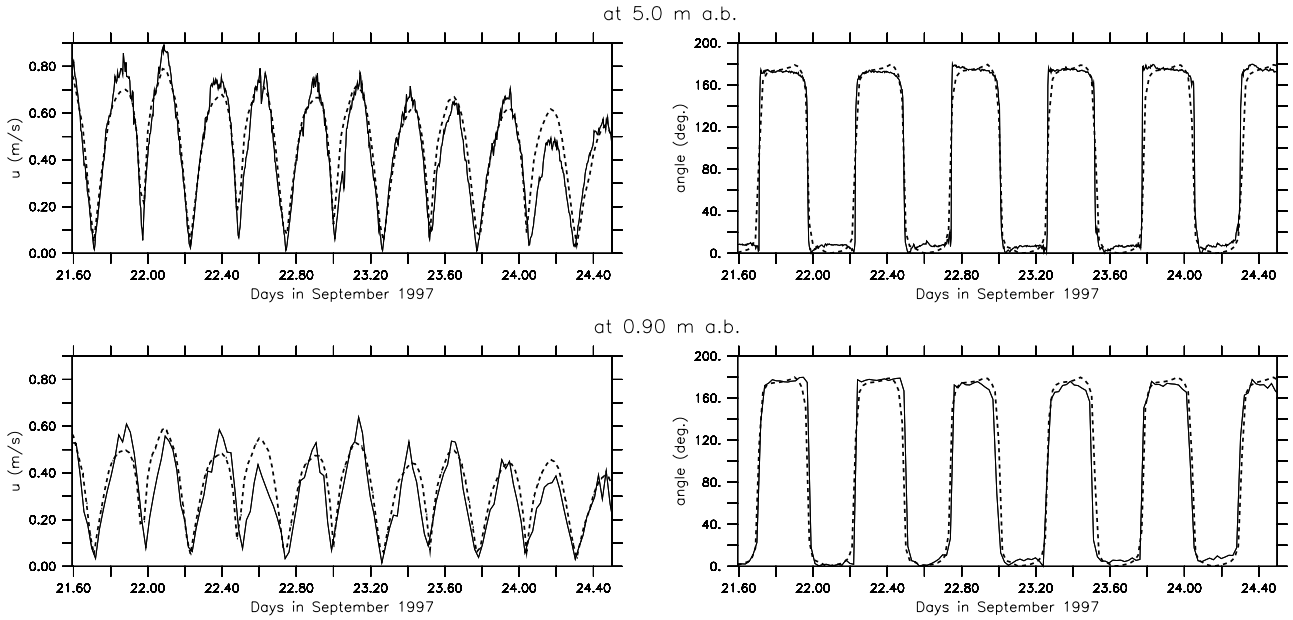

Figure 6. Measured (black line) and computed (dotted line) time series of the speed and direction (clockwise from the north) at 0.9 and 5 m above the bottom at the Hardelot site.

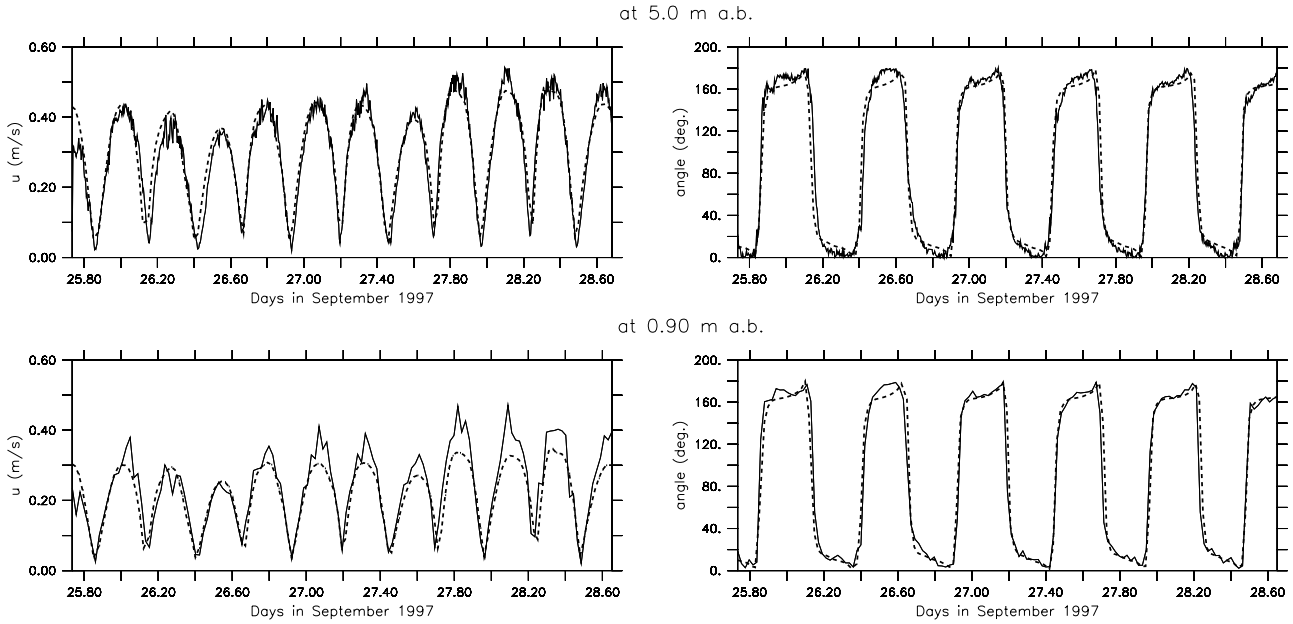

Figure 7. Measured (black line) and computed (dotted line) time series of the speed and direction (clockwise from the north) at 0.9 and 5 m above the bottom at the Merlimont site.

in Figure 8. Except around the missing data at the Hardelot site and during the second half of the measurement period at the Merlimont site characterized by an underestimation of turbulent kinetic energy predictions consistent with current velocities predictions previously mentioned, the model is in fairly good agreement with measurements. This local statement at 0.9 m above the bottom can be generalized to the four elevations which are within the near-bed constant stress layer.

3.4.3. SSC Predictions

[25] The SSC computations are performed with a resuspension parameter $\gamma_0 = 5.5 \times 10^{-4}$. This falls in the range $[10^{-5}; 10^{-3}]$ obtained by compiling the values suggested by *Dyer* [1980], *Wiberg and Smith* [1983], *Drake and Cacchione* [1989] and *Vincent and Green* [1990] on the continental shelf. The time series of total SSC at the Hardelot site is fairly well predicted by the model (Figure 9). In particular, a good agreement is observed for the relative phase and magnitude of successive semidiurnal peaks exhibiting a flood/ebb asymmetry and decreasing from spring to neap tides. Minima of SSC around slack waters are found to be overestimated by a factor of two at the beginning of the measurement period under spring tide conditions. This overprediction diminishes progressively as neap tides approach.

[26] Model predictions class by class reveal very specific resuspension responses. First of all, we notice that only the first three grain size classes with diameters $d_1 = 25$ μm, $d_2 = 75$ μm and $d_3 = 150$ μm contribute to the total SSC at the Hardelot site. The time series of SSC of the finest class ($d_1 = 25$ μm) indicates a semidiurnal evolution with ebb peaks superimposed on a "background" SSC which decreases from 18 mg l^{-1} to 10 mg l^{-1} with the spring/neap tide cycle. The time series of SSC of the two coarser classes ($d_2 = 75$ μm and $d_3 = 150$ μm) exhibit a quarter-diurnal variation characterized by a zero background concentration resulting from active sedimentation rates and a flood/ebb asymmetry which grows with the grain size diameter. These two coarse classes are found to govern the temporal variation of the total SSC signal. The SSC signal of the finest class ($d_1 = 25$ μm) contributes only to reduce the flood/ebb asymmetry. Finally, a close inspection of SSC signals shows a phase lag of less than 1 h for the first class ($d_1 = 25$ μm) and 30 min for the second class ($d_2 = 75$ μm) with respect to the bottom local

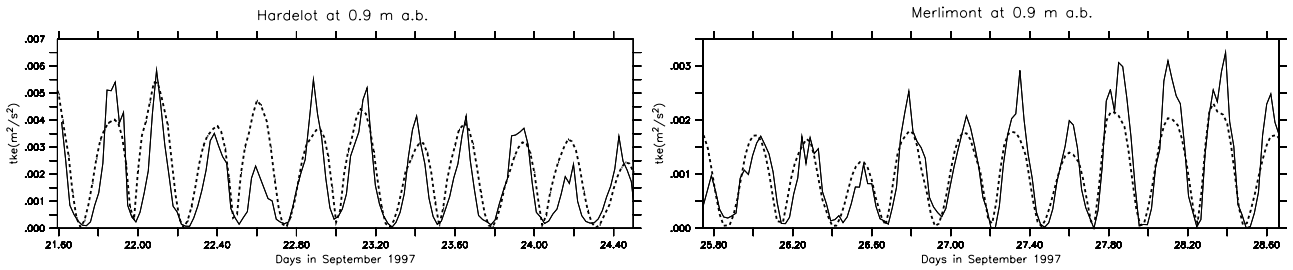

Figure 8. Measured (black line) and computed (dotted line) time series of the turbulent kinetic energy at 0.9 m above the bottom at the Hardelot and Merlimont sites.

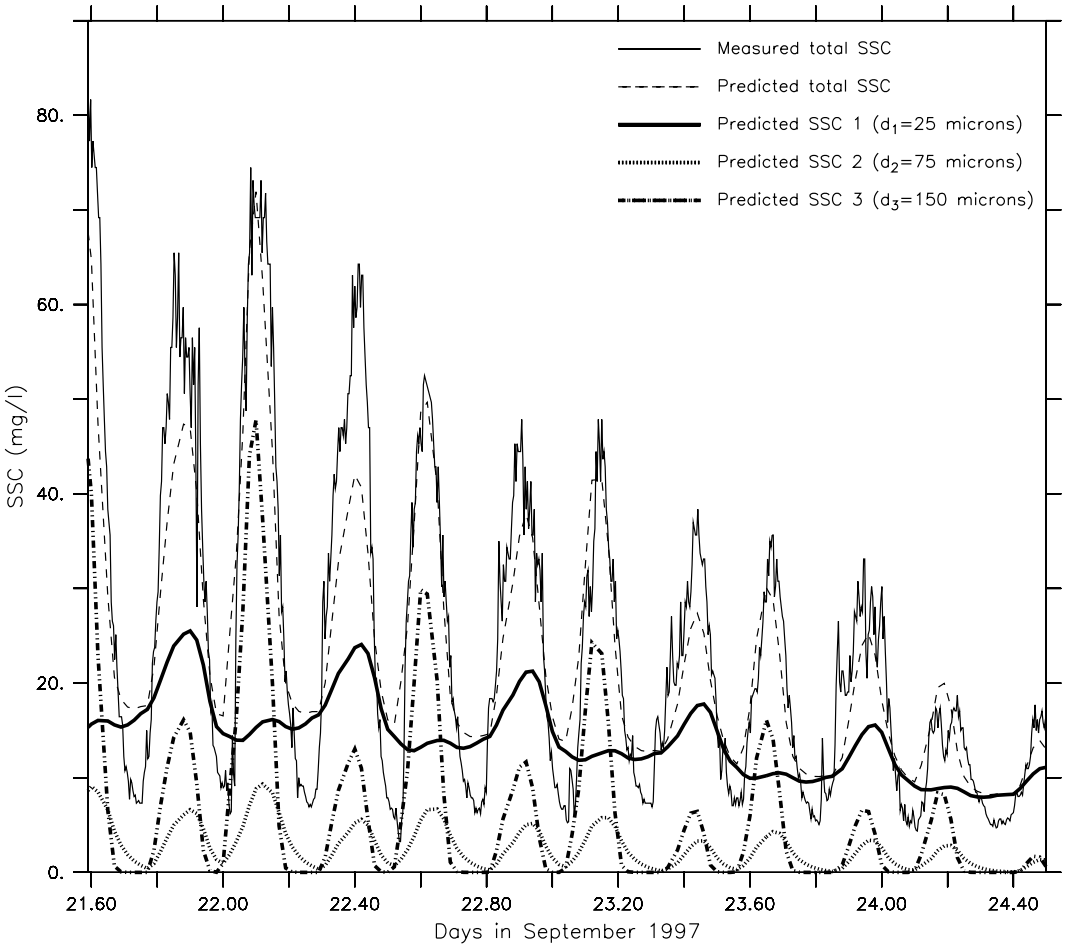

Figure 9. Measured and computed time series of the total SSC and the SSC of the first three classes with diameters $d_1 = 25\mu$m, $d_2 = 75\ \mu$m, and $d_3 = 150\ \mu$m involved in suspension at 5 m above the bottom at the Hardelot site.

shear stress. This feature suggests remote advective and diffusive effects which will be discussed in section 4.

4. Discussion

[27] SSC signals of the first three grain size classes are further investigated spatially in the surroundings of the Hardelot site. Figure 10 displays the predicted maps of the skin friction velocity u_{*skin} and the SSC of the first three grain size classes ($d_1 = 25\ \mu$m, $d_2 = 75\ \mu$m and $d_3 = 150\ \mu$m) at 5 m above the bottom at four moments during the first tidal cycle of 22 September 1997. During the flood peak (T2), characterized by a strong positive south-north gradient of bottom friction, a cloud of silts ($d_1 = 25\ \mu$m) resuspension with a kernel exceeding 30 mg l^{-1} develops on the nearshore belt of bottom silty sands (Figure 5a). This cloud spreads northeast and east of the Hardelot site and is bounded north by cape Alprech. At the same time, high resuspensions of fine sand ($d_3 = 150\ \mu$m) between 40 and 70 mg l^{-1} occur in the north of the Hardelot site. This event is to be related with skin friction velocities exceeding 2.2 cm s^{-1} and significant supplies of sedimentary materials (Figure 5c). Until the slack water, the cloud of silts is subject to an advection northward with a deflection offshore by the cape Alprech and a spreading by the horizontal dispersion. At the time of the slack water (T3), the water at 5 m above the bottom is free of fine sands while the cloud of suspended silts is maintained with lessened magnitude because of past dispersion, reduced erosion and sedimentation. During the ebb peak (T4), the cloud of suspended silts moves slightly southward transporting remote suspended sediment at the Hardelot site. This cloud strengthens in SSC magnitude up to 32 mg l^{-1} by resuspension of bottom silty sand at the outer edge of the nearshore belt (Figure 5a). At the same time, suitable excess of shear stress and bottom sediment supply conditions allow a cloud of resuspension of fine sands reaching about 15 mg l^{-1} to form in the vicinity of the Hardelot site. The

Figure 10. Predicted skin friction velocity u_{*skin} and SSC of the first three classes at 5 m above the bottom in the surroundings of the Hardelot site on 22 September 1997: the initiation of the flood at 0112 UT (T1), the peak of total SSC during the flood at 0250 UT (T2), the initiation of the ebb at 0820 UT (T3), and the peak of total SSC during the ebb at 0950 UT (T4). Notice that areas where $u_{*skin} > 3$ cm s^{-1} are colored in black.

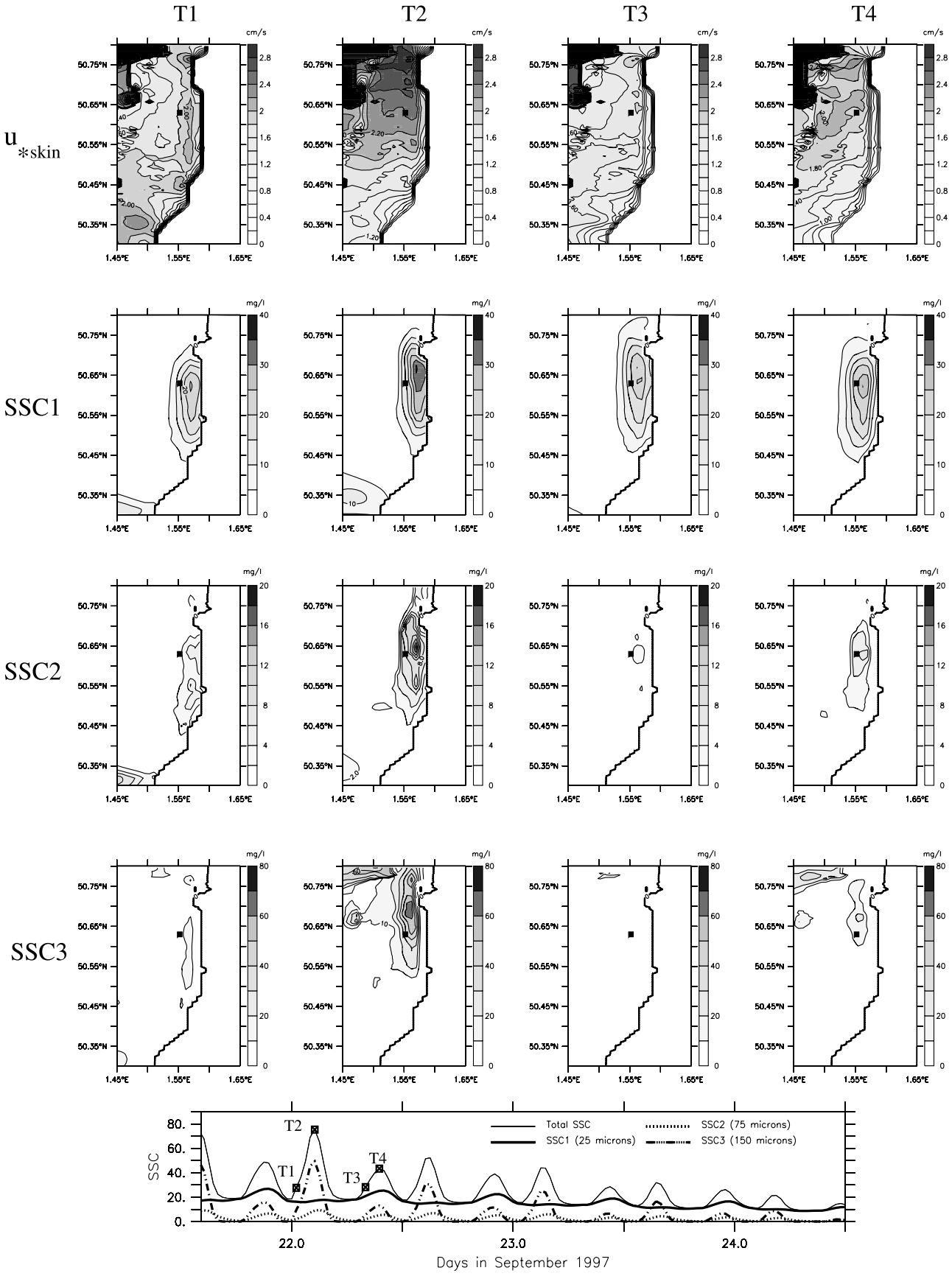
T1
T2
T3
T4
u*skin
SSC1
SSC2
SSC3
cm/s
mg/l
50.75°N
50.65°N
50.55°N
50.45°N
50.35°N
1.45°E
1.55°E
1.65°E
SSC
Total SSC
SSC1 (25 microns)
SSC2 (75 microns)
SSC3 (150 microns)
22.0
23.0
24.0
Days in September 1997

Figure 10

evolution of resuspension of the intermediate class of very fine sands (d_2 = 75 μm) at the four different key moments of the tidal cycle exhibits a similar behavior to the one of fine sand (d_3 = 150 μm). This confirms the findings from the time series of SSC of the three grain size classes at the Hardelot site (Figure 9).

5. Conclusions

[28] A three-dimensional hydrodynamics and multicomponent sediment transport model was implemented with realistic bottom sediment compositions in order to quantify tidal-induced suspended transport including erosion, advection, dispersion and settling in the eastern English Channel. Predicted time series of hydrodynamic components over the water column show a fairly good agreement at the two measuring points of Hardelot and Merlimont in the south of Boulogne-sur-Mer. The model is also able to predict the total SSC observed at the Hardelot site. The contributions of the different classes highlight the intricate effects of the spatial heterogeneity of bottom sediments, the bathymetry and the coastline geometry on suspended sediment transport in the near-field area of the experimental site of Hardelot.

[29] The present study is restricted to resuspensions issued from the bottom of the computational domain. Further developments will consist in incorporating fluxes of fresh waters and sediment through the open boundaries, including rivers, particularly those from the Seine and the Thames. A second perspective is the implementation in the model of the physical properties of cohesive sediments (erosion, flocculation-breakup and settling) to account for muddy sediments in low-energy areas and/or estuaries (e.g., bay of Seine).

[30] These developments in combination with advanced comparisons of the model results with complementary in situ measurements of multicomponent SSC using laser diffraction sensor (e.g., LISST-100 manufactured by Sequoia Scientific, Inc.) and ocean color satellite images (e.g., SPOT, SeaWiFS, Modis) would allow a better estimate of sediment fluxes through the Dover Strait.

[31] **Acknowledgments.** The authors are particularly grateful to Louis Cabioch for giving us access to RCP 378 Benthos de la Manche data and to José Ozer (Management Unit of the North Sea Mathematical Models) for providing 21 tidal harmonic constituents extracted from a COHERENS run over the northwest European continental shelf. Computations were performed at the computer center CAPARMOR. The present paper is a contribution to the Institut Universitaire Européen de la Mer (CETMEF-IUEM) joint research programme Mesure et Modélisation des Processus Hydrodynamiques et Hydro-Sédimentaires Littoraux (MEMPHYS).

References

Augris, C., P. Clabaut, S. Dewez, and J. P. Auffret (1987), Surficial sediments map off Boulogne-sur-Mer (France), scale 1:43,600, Inst. Fr. de Rech. pour l'Explor. de la Mer, Issy-les-Moulineaux, France.

Barenblatt, G. T. (1953), Motion of suspended particles in a turbulent flow, *Prikl. Mat. Mekh.*, *17*(3), 261–274.

Blumberg, A. F., and L. H. Kantha (1985), Open boundary conditions for circulation models, *J. Hydraul. Eng.*, *11*, 237–255.

Blumberg, A. F., and G. L. Mellor (1987), A description of a three-dimensional coastal ocean circulation model, in *Three-Dimensional Coastal Ocean Models, Coastal and Estuarine Sci.*, vol. 4, edited by N. S. Heaps, pp. 1–16, AGU, Washington, D. C.

Cabioch, L., F. Gentil, R. Glacon, and C. Retière (1977), Le macrobenthos des fonds meubles de la Manche: distribution générale et écologie, in *Biology of Benthic Organims*, edited by B. F. Keegan, P. O. Ceidigh, and P. J. Caston, pp. 115–128, Pergamon, Oxford, U. K.

Celik, I., and W. Rodi (1988), Modelling suspended sediment transport in non-equilibrium situations, *J. Hydraul. Eng.*, *10*(114), 1119–1157.

Celik, I., and W. Rodi (1991), Suspended sediment-transport capacity for open channel flow, *J. Hydraul. Eng.*, *2*(117), 191–204.

Chapalain, G., and L. Thais (2000), Tide, turbulence and suspended sediment modelling in the eastern English Channel, *Coastal Eng.*, *41*, 295–316.

Chapalain, G., L. Thais, and H. Smaoui (1999), Modeling of a tidal bottom boundary layer with suspended sediment, *Hydrobiologia*, *414*, 1–12.

Drake, D. E., and D. A. Cacchione (1989), Estimates of the suspended sediment reference concentration (c_a) and resuspension coefficient (γ_0) from near-bed observations on the California shelf, *Cont. Shelf Res.*, *9*, 51–64.

Dyer, K. R. (1980), Current velocity profiles over rippled bed and the threshold of movement of sand, *Estuarine Coastal Mar. Sci.*, *10*, 181–189.

Eisma, D., and J. Kalf (1979), Distribution and particle size of suspended matter in the southern bight of the North Sea and the eastern channel, *Neth. J. Sea Res.*, *13*(2), 298–324.

Flather, R. A. (1976), A tidal model of the northwest european continental shelf, *Mem. Soc. R. Sci. Liege*, *97*, 141–164.

Grant, W. D., and S. M. Glenn (1983), Continental shelf bottom boundary layer model, vol. I, Theoretical model development, *Rep. PR-153-126*, 163 pp., Am. Gas Assoc., Washington, D. C.

Grochowski, N. T. L., and M. B. Collins (1994), Wave activity on the seabed of the English Channel, *J. Mar. Biol. Assoc. U. K.*, *74*, 739–742.

Grochowski, N. T. L., M. B. Collins, S. R. Boxall, and J.-C. Salomon (1993a), Sediment trasnport predictions for the English Channel, using numerical models, *J. Geol. Soc.*, *150*, 683–695.

Grochowski, N. T. L., M. B. Collins, S. R. Boxall, J.-C. Salomon, M. Breton, and R. Lafite (1993b), Sediment transport pathways in the eastern channel, *Oceanol. Acta*, *16*, 531–537.

Guillou, N. (2007), Rôles de l'hétérogénéité des sédiments de fonds et des interactions houle-courant sur l'hydrodynamique et la dynamique sédimentaire en zone subtidale—Applications en Manche orientale et à la pointe de la Bretagne, doctoral thesis, 469 pp., Univ. de Bretagne Occidentale, Brest, France.

Hess, K. W. (1986), Numerical model of circulation in Chesapeake Bay and the continental shelf, *NOAA Tech. Memo. NESDIS/AISC 6*, 47 pp., Natl. Environ. Satell., Data and Infor. Serv., U.S. Dep. of Commer., Silver Spring, Md.

Kenyon, N. H., and A. H. Stride (1970), The tide-swept continental shelf sediments between the Shetland Isles and France, *Sedimentology*, *14*, 159–173.

Lafite, R., S. Shimwell, N. Grochowski, J. P. Dupont, L. Nash, J. C. Salomon, L. Cabioch, M. Collins, and S. Gao (2000), Suspended particulate matter fluxes through the Straits of Dover, English Channel: Observations and modelling, *Oceanol. Acta*, *23*(6), 687–699.

Launder, B. E., and D. B. Spalding (1974), The numerical computation of turbulent flows, *Comput. Methods Appl. Mech. Eng.*, *3*, 269–289.

Lavelle, J. W., H. O. Mofjeld, and E. T. Baker (1984), An in situ erosion rate for fine-grained marine sediment, *J. Geophys. Res.*, *89*, 6543–6552.

Leprêtre, A., G. Chapalain, and P. Carpentier (2006), Une méthode d'interpolation des caractéristiques granulométriques des sédiments superficiels, *Bull. Soc. Geol. Fr.*, *177*(2), 89–95.

Li, M. Z. (1994), Direct skin friction measurements and stress partitioning over moveable sand ripples, *J. Geophys. Res.*, *99*, 791–799.

Lick, W. (1982), Entrainment, deposition and transport of fine-grained sediments in lakes, *Hydrobiologia*, *91*, 31–40.

Lumley, J. L. (1978), Two-phase and non-Newtonian flows, in *Turbulence, Topics in Appl. Phys.*, vol. 12, pp. 289–324, Springer, Berlin.

Luyten, P. J., E. Deleersnijder, J. Ozer, and K. G. Ruddick (1996), Presentation of a family of turbulence closure models for stratified shallow water flows and preliminary application to the Rhine outflow region, *Cont. Shelf Res.*, *16*, 101–130.

Luyten, P. J., J. E. Jones, R. Proctor, A. Tabor, P. Tett, and K. Wild-Aden (1999a), COHERENS: A Coupled Hydrodynamical-Ecological Model for Regional and Shelf Seas: User documentation, *Rep. MAS3-CT97-088*, 911 pp., Manage. Unit of the Math. Models of the North Sea, Brussels.

Luyten, P. J., J. E. Jones, R. Proctor, A. Tabor, P. Tett, and K. Wild-Aden (1999b), COHERENS: A Coupled Hydrodynamical-Ecological Model for Regional and Shelf Seas: Model applications—North Sea case study, *Rep. MAS3-CT97-088*, 211 pp., Manage. Unit of the Math. Models of the North Sea, Brussels.

Rodi, W. (1984), *Turbulence Models and Their Application in Hydraulics*, 2nd ed., 104 pp., Int. Assoc. for Hydraul. Res., Delft, Netherlands.

Salomon, J.-C., M. Breton, and P. Guegueniat (1993), Computed residual flow through the Dover Strait, *Oceanol. Acta*, *16*, 449–455.

Schepetkin, A. F., and J. C. McWilliams (2005), The Regional Oceanic Modeling System (ROMS): A split-explicit, free-surface, topography-following-coordinate oceanic model, *Ocean Modell.*, *9*, 347–404.

Service Hydrographique et Océanographique de la Marine (1973), Courants de marée de Dunkerque à Brest, Imprimerie Natl., Paris.
Sheng, Y. P. (1983), Mathematical modeling of three-dimensional coastal currents and sediment dispersion: Model development and application, *Tech. Rep., CERC-83-2*, 297 pp., Chief of Eng., U.S. Army, Washington, D. C.
Smagorinsky, J. (1963), General circulation experiments with the primitive equations: I. The basic experiments, *Mon. Weather Rev.*, *91*, 99–164.
Smith, J., and S. R. McLean (1977), Spatially averaged flow over a wavy surface, *J. Geophys. Res.*, *82*, 1735–1746.
Soo, S. L. (1967), *Fluid Dynamics of Multiphase Systems*, 524 pp., Blaisdell, Waltham, Mass.
Soulsby, R. (1997), *Dynamics of Marine Sands*, 249 pp., T. Telford, London.
Soulsby, R. L., and B. L. S. A. Wainwright (1987), A criterion for the effect of suspended sediment on near bottom velocity profiles, *J. Hydraul. Res.*, *25*, 341–355.
Soulsby, R. L., and R. J. S. W. Whitehouse (1997), Threshold of sediment motion on coastal environments, paper presented at Pacific Coasts and Ports '97 Conference, Univ. of Canterbury, Christchurch, New Zealand.
Souza, A. J., J. T. Holt, and R. Proctor (2007), Modelling SPM on the NW European shelf seas, *Coastal Shelf Sediment Transp.*, *274*, 147–158.
Stride, A. H. (1963), Current-swept sea floors near the southern half of Great Britain, *J. Geol. Soc. London*, *119*, 175–199.
Stride, A. H., R. H. Belderson, and N. H. Kenyon (1972), Longitudinal furrows and depositional sand bodies of the English Channel, in Colloque sur la géologie de la Manche, *Mem. BRGM*, *79*, 233–240.
Van Rijn, L. C. (1986), Mathematical modelling of suspended sediment in non-uniform flows, *J. Hydraul. Eng.*, *112*, 433–455.
Van Rijn, L. C. (1993), *Principles of Sediment Transport in Rivers*, Estuaries and Coastal Seas, Aqua, Amsterdam.
Vaslet, D., C. Larsonneur, and J. P. Auffret (1979), Map of the surficial sediments of the English Channel, scale 1:500,000, Bur. de Rech. Géol. et Minières, Orléans, France.
Vincent, C. E., and O. M. Green (1990), Field measurements of the suspended sand concentration profiles and fluxes, and of the resuspension coefficient γ_0 over a rippled bed, *J. Geophys. Res.*, *95*, 15,591–15,601.
Wiberg, P. L., and J. D. Smith (1983), A comparison of field data and theoretical models for wave-current interactions at the bed of the continental shelf, *Cont. Shelf Res.*, *2*, 147–162.
Wooding, R. A., E. F. Bradley, and J. K. Marshall (1973), Drag due to regular arrays of roughness elements of varying geometry, *Boundary Layer Meteorol.*, *5*, 285–308.
Yalin, M. S. (1985), On the determination of ripple geometry, *J. Hydraul. Eng.*, *8*(111), 1148–1155.

G. Chapalain and N. Guillou, Laboratoire Génie Côtier et Environnement, Département Environnement Littoral et Cours d'Eau, Centre d'Etudes Techniques Maritimes et Fluviales, Technopôle Brest-Iroise, BP 5, F-29280 Plouzané, France. (georges.chapalain@univ-brest.fr; nicolas.guillou@developpement-durable.gouv.fr)

L. Thais, Laboratoire de Mécanique de Lille, UMR 8107, USTL, Polytech'Lille, CNRS, Avenue Paul Langevin, F-59655 Villeneuve d'Ascq CEDEX, France. (laurent.thais@polytech-lille.fr)